Figure S1

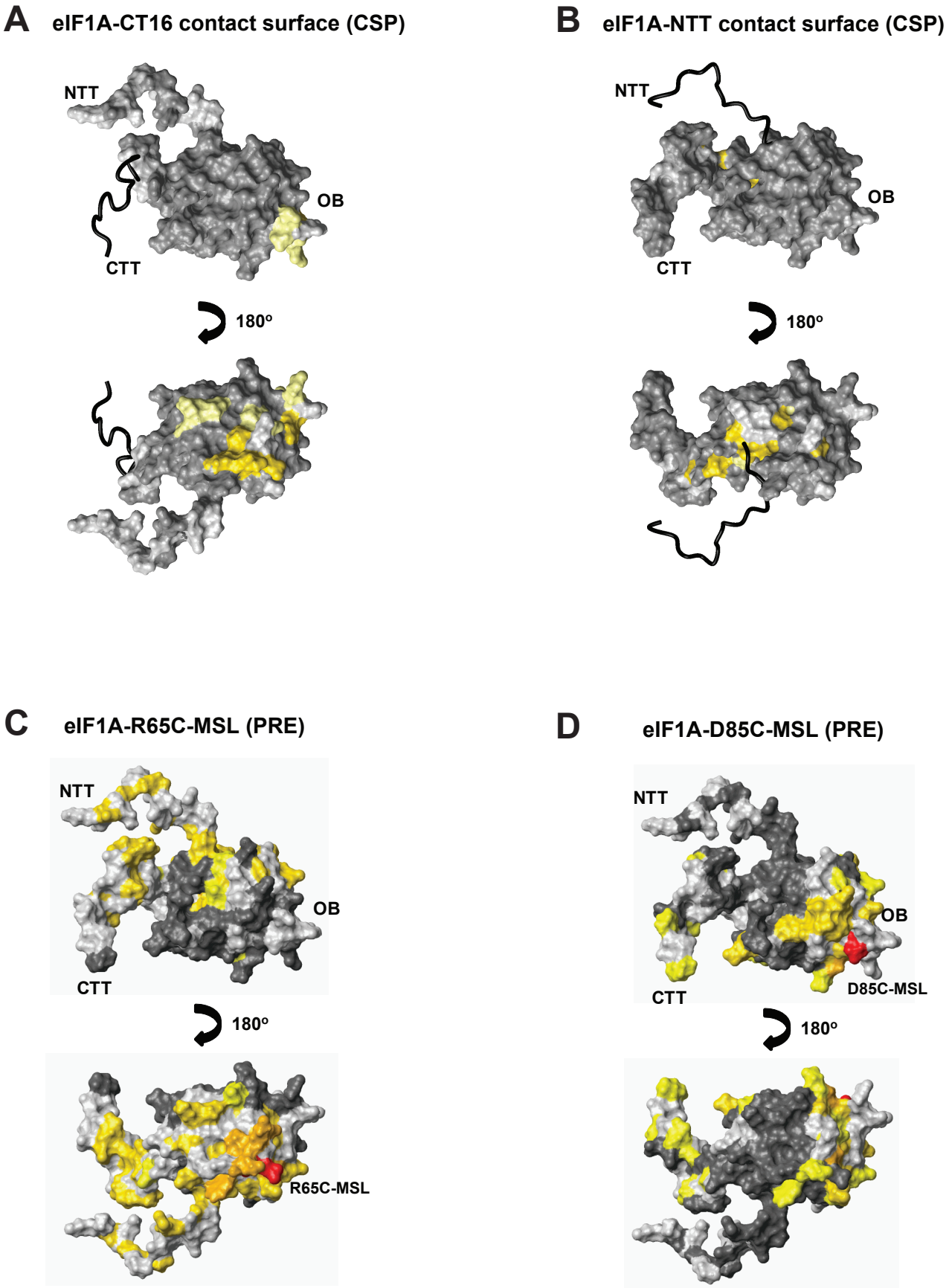
A
eIF1A-CT16 contact surface (CSP)
NTT
OB
CTT
180°
B
eIF1A-NTT contact surface (CSP)
NTT
OB
CTT
180°
C
eIF1A-R65C-MSL (PRE)
NTT
OB
CTT
180°
R65C-MSL
D
eIF1A-D85C-MSL (PRE)
NTT
OB
CTT
D85C-MSL
180°

Figure S1. Intramolecular interactions within eIF1A

(A) eIF1A-OB domain surfaces affected by eIF1A-CT16 deletion in CSP assay. eIF1A is in surface representation, except the CT16, which is shown as wire. Affected residues are colored yellow (smaller effects) and dark yellow (larger effects); Residues with no significant changes are dark grey; residues that could not be analyzed are light grey. **(B)** eIF1A surfaces affected by the eIF1A-NTT deletion in CSP assay. Affected residues are colored yellow (smaller effects) and dark yellow (larger effects). eIF1A is in surface representation, except the NTT, which is shown as wire. **(C)** PRE effects on eIF1A residues in OPM-labeled $eIF1A_{R65C}$. Affected residues are colored from yellow (smaller effects) to orange (larger effects). The position of the OPM label, residue 65, is colored red. **(D)** PRE effects on eIF1A residues in OPM-labeled $eIF1A_{D85C}$. Affected residues are colored from yellow (smaller effects) to orange (larger effects). The position of the OPM label, residue 85, is colored red.

A NMR spectra of $^{15}N/^{2}H$-eIF5B-D4 in the absence (**black**) and presence of eIF1A (**red**)

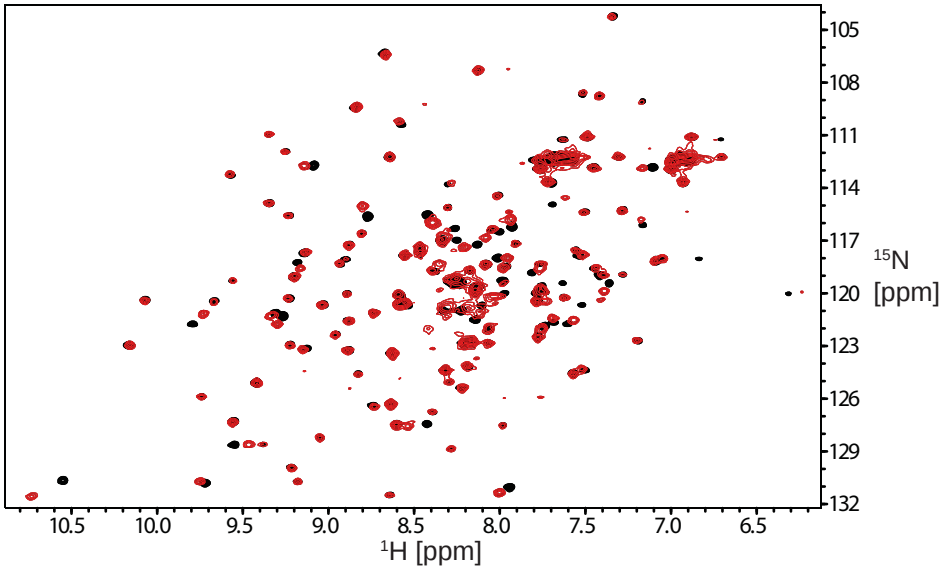

B NMR spectra of $^{15}N/^{2}H$-eIF5B-D4 in the absence (**black**) and presence of eIF1A-CTT (**red**)

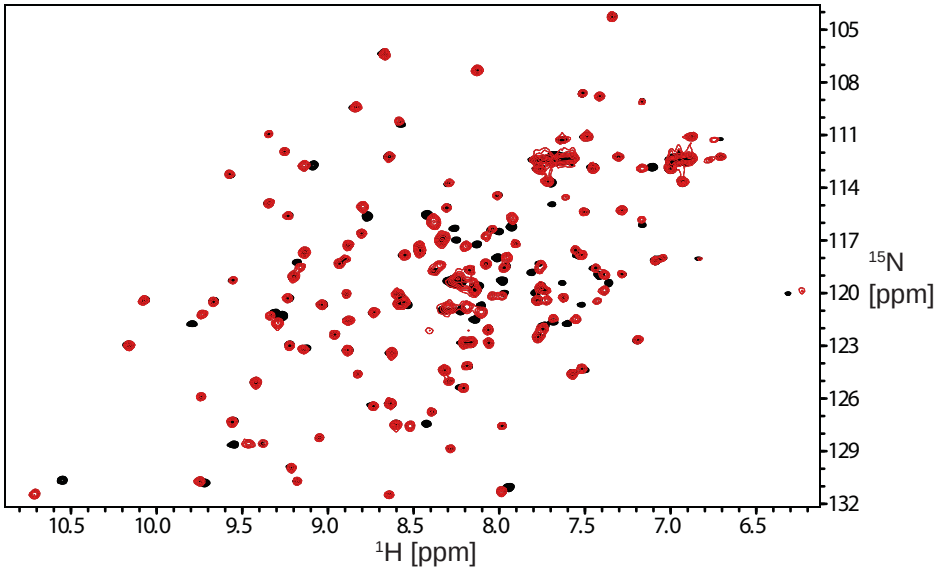

C NMR spectra of $^{15}N/^{2}H$-eIF5B-D4 in the absence (**black**) and presence of eIF1A-CT16 (**red**)

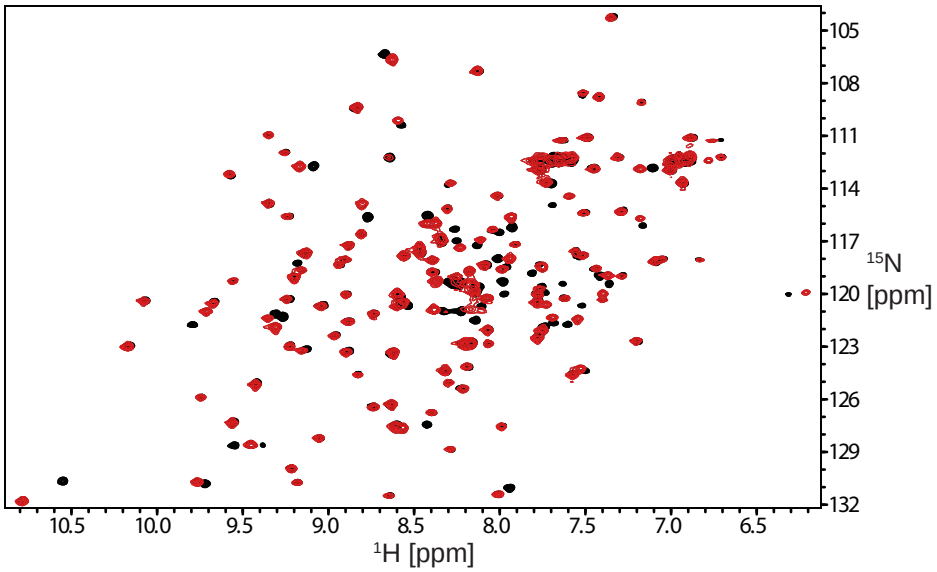

Figure S2. eIF1A-CT16 is sufficient for binding to eIF5B-D4

(A) Overlay of NMR spectra of $^{15}N/^{2}H$-eIF5B-D4 in the absence (black) and presence of eIF1A (red). **(B)** Overlay of NMR spectra of $^{15}N/^{2}H$-eIF5B-D4 in the absence (black) and presence of eIF1A-CTT (red). **(C)** Overlay of NMR spectra of $^{15}N/^{2}H$-eIF5B-D4 in the absence (black) and presence of eIF1A-CT16 (red). Essentially the same set of peaks (and thus, eIF5B-D4 residues) are affected by eIF1A, eIF1A-CTT, and eIF1A-CT16 binding in panels *(A)*, *(B)*, and *(C)*, respectively.

A NMR spectra of $^{15}N/^{2}H$-eIF1A$_{\Delta C}$ in the absence (**black**) and presence (**red**) of eIF5B-D123, processed identically (left) and the spectrum of the complex run longer (right)

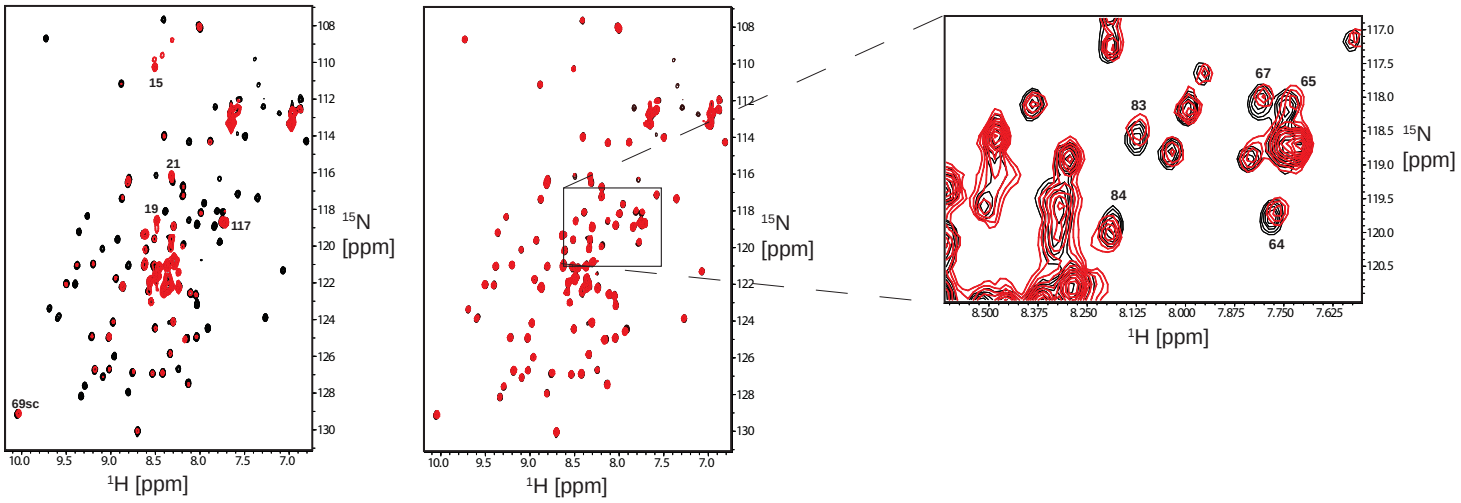

B NMR spectra of $^{15}N/^{2}H$-eIF1A$_{\Delta C}$ in the absence (**black**) and presence (**red**) of eIF5B-D34

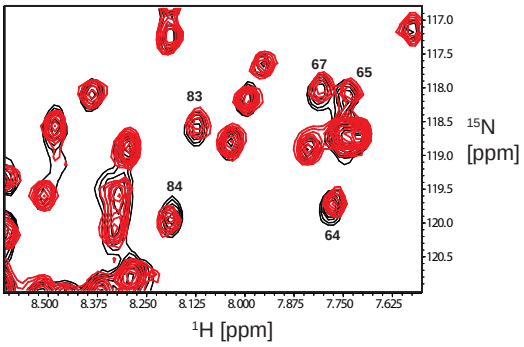

C NMR spectra of ^{15}N-eIF1A$_{\Delta C}$ in the absence (**black**) and presence (**red**) of eIF5B-D3

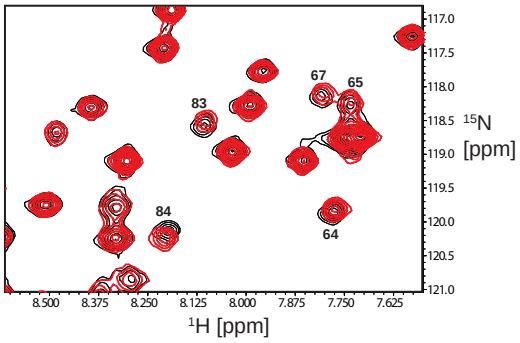

D NMR spectra of ^{15}N-eIF1A in the absence (**black**) and presence (**red**) of eIF5B-D34

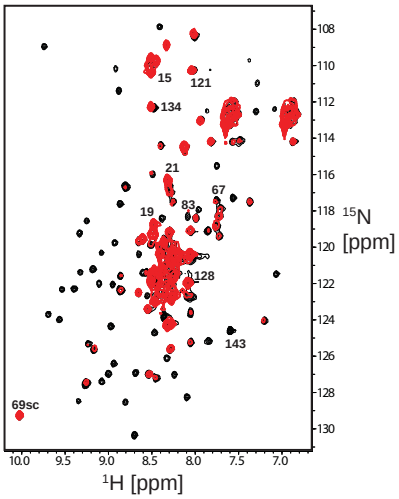

Figure S3. eIF5B-D3 is sufficient for binding to eIF1A-OB

(A) ***Left***, overlay of NMR spectra of $^{15}N/^{2}H$-eIF1A$_{\Delta C}$ in the absence (black) and presence of eIF5B-D123 (red). The spectra are processed and displayed identically. Select peaks from the NTT, as well as other peaks that remain visible in the presence of eIF5B-D123 are labeled. Loss of most peaks, except those belonging to residues in the eIF1A-NTT and other flexible regions, indicates formation of a large complex, in which the NTT remains dynamic. ***Right***, the spectrum of the complex run longer and displayed with lower cutoff allows observing peaks belonging to the folded OB domain. Chemical shift changes can be better seen in the inset. **(B)** Overlay of NMR spectra of $^{15}N/^{2}H$-eIF1A$_{\Delta C}$ in the absence (black) and presence of eIF5B-D34 (red). Only the region shown in the inset in panel *(A)* is shown. Note that the same set of peaks move in a similar way in panels *(A)* and *(B)*, indicating that D3, which is common for both eIF5B constructs, is responsible for the binding. **(C)** Overlay of NMR spectra of ^{15}N-eIF1A$_{\Delta C}$ in the absence (black) and presence of eIF5B-D3 (red). Only the region shown in the inset in panel *(A)* is shown. Note that the same set of peaks move in a similar way in panels *(A)*, *(B)* and *(C)*, indicating that eIF5B-D3 is sufficient for binding to eIF1A-OB. **(D)** Overlay of NMR spectra of ^{15}N-eIF1A in the absence (black) and presence of eIF5B-D34 (red). The spectrum of the complex is run longer and displayed with lower cutoff, which allows observing some of the peaks belonging to the folded OB domain, while peaks belonging to flexible segments appear stronger than in the spectrum of the free protein. Selected peaks the remain visible in the complex (red) are labeled: residues 15, 19, and 21 in the NTT; residues 67, 83 and the side chain NH of 69 in the OB; and residues 121,128, and 134 in the CTT. The peak corresponding to the C-terminal residue 143, which is not visible in the complex due to binding to eIF5B-D4, is also labeled. Severe loss of signal is observed in the eIF1A C-terminus (binding to eIF5B-D4) and the eIF1A-OB domain (binding to eIF5B-D3). The NTT as well as most of the CTT remain flexible. Chemical shift changes are also observed in visible peaks belonging to both the CTT (e.g. 134) and the OB (e.g. 67 and 83).

A PREs in eIF5B-D34 in complex with eIF1A-D85C-OPM

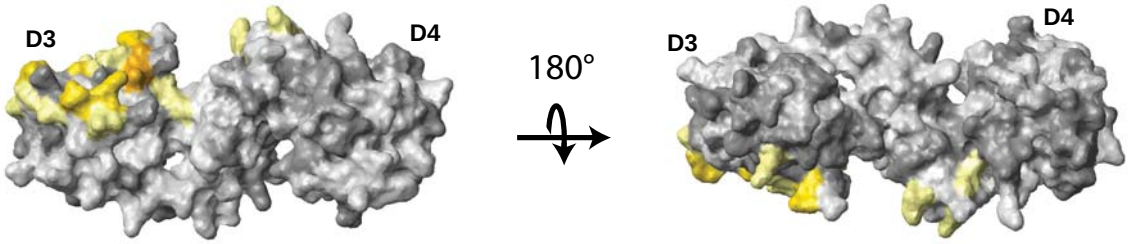

B PREs in eIF5B-D34 in complex with eIF1A-D137C-OPM

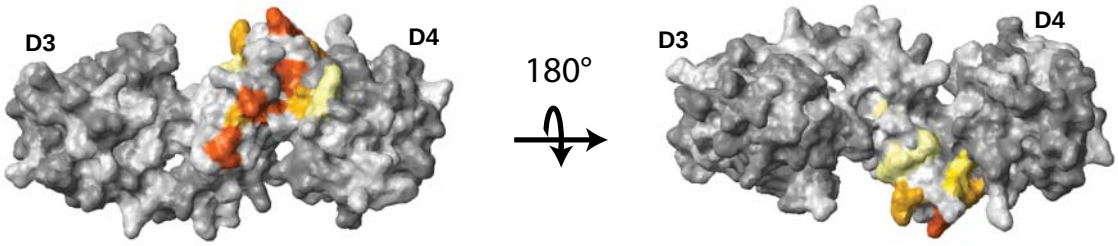

C Model for the eIF5B-D34:eIF1A complex in solution

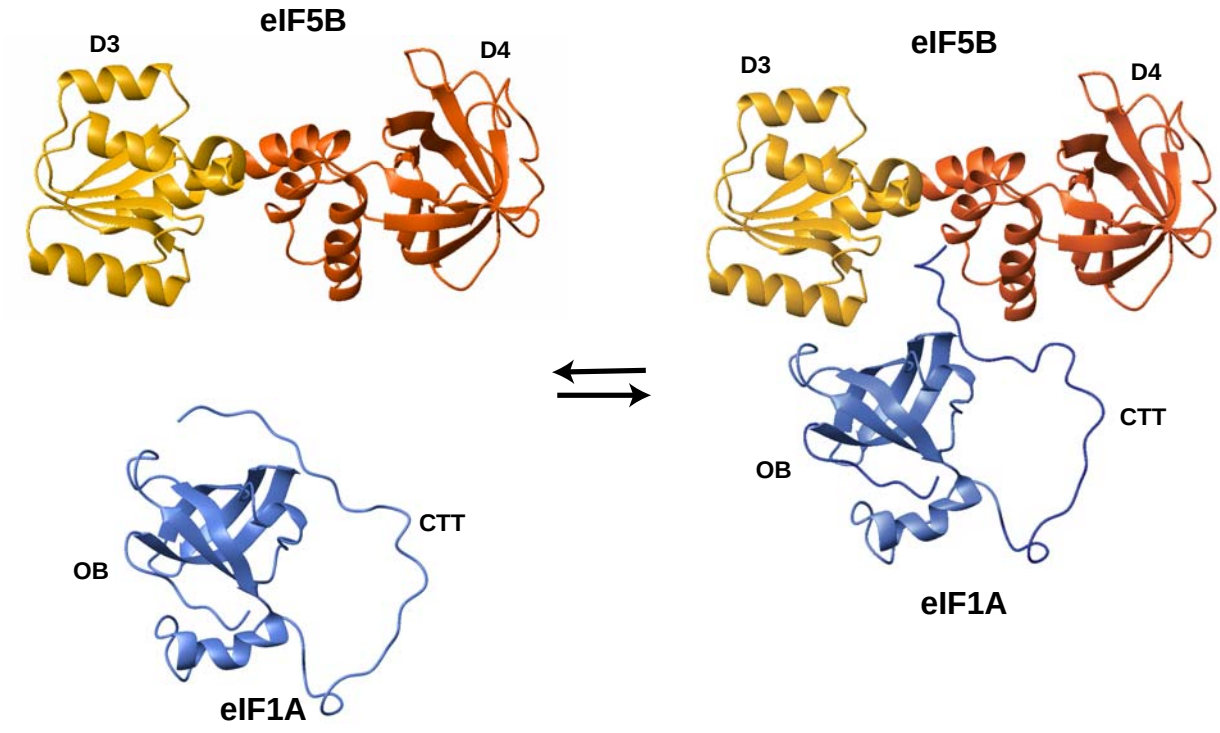

Figure S4. Interactions between eIF5B-D34 and eIF1A

(A) PRE effects on eIF5B-D34 residues in complex with OPM-labeled eIF1A$_{D85C}$. In the left panel, eIF5B-D34 is in the same orientation as in ***Fig. 5D***. Affected residues are colored from yellow (smaller effects) to orange (larger effects). **(B)** PRE effects on eIF5B-D34 residues in complex with OPM-labeled eIF1A$_{D137C}$. Affected residues are colored from yellow (smaller effects) to dark orange (larger effects). **(C)** Model for the structure of the eIF5B-D34:eIF1A complex in equilibrium with the free proteins.

A **Modeling eIF1A into the eIF5B:80S IC complex**

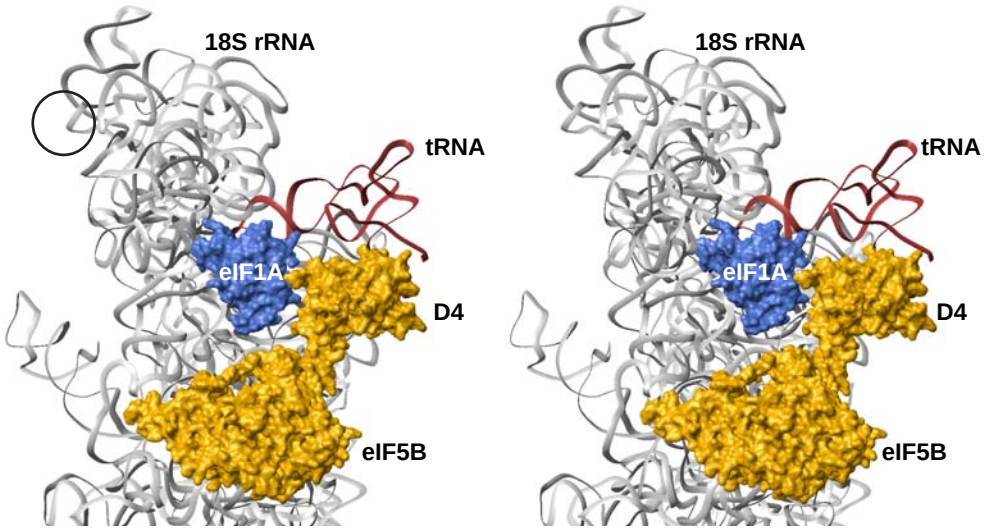

B **Comparison of the position of eIF5B-D4 in 80S IC to that of eIF2 in open 48S PIC**

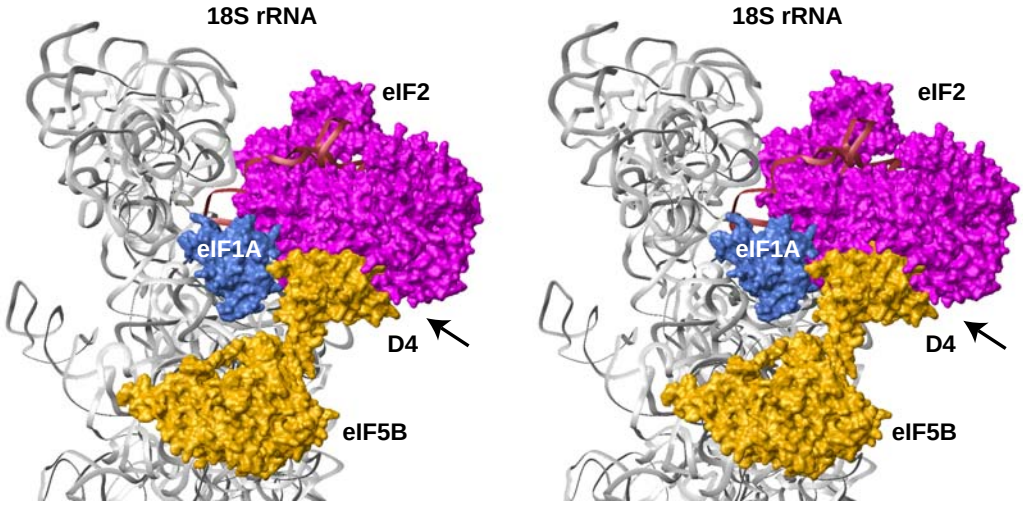

C **Comparison of the position of eIF5B-D4 in 80S IC to that of eIF2 in closed 48S PIC**

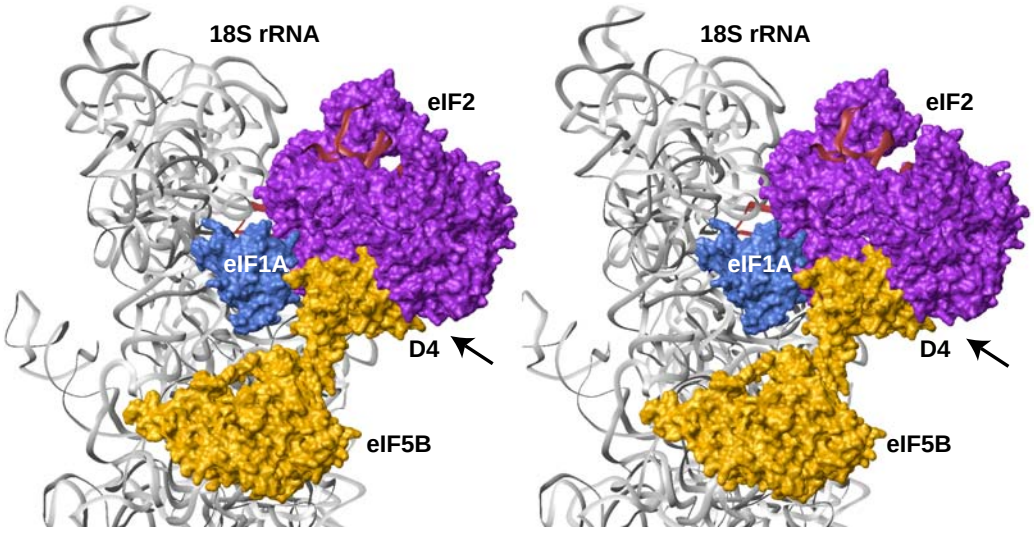

Figure S5. Modeling eIF1A and eIF5B on the ribosome

(A) Modeling eIF1A into the eIF5B:80S IC, in cross-eye stereo. The model was obtained by aligning the 18S rRNA from the open 48S PIC (3jaq.pdb)(Llacer et al. 2015) and the eIF5B:80S IC pre-like state (4ujd.pdb)(Yamamoto et al. 2014). Only the 18S rRNA, eIF5B, Met-tRNA$_i$ from the 80S IC, and eIF1A from the 48S PIC are shown. eIF1A and eIF5B-D4 are in close proximity, with no steric clashes, indicating that eIF1A-OB and eIF5B-D4 can contact each other in the 80S IC. **(B)** Modeling eIF5B into the open 48S PIC, in cross-eye stereo. The model was obtained as in panel *(A)*. Only the 18S rRNA and eIF5B from the 80S IC, and Met-tRNA$_i$, eIF2, and eIF1A from the 48S PIC are shown. A steric clash between eIF2 and eIF5B-D4 is evident (marked by arrows), indicating that eIF5B-D4 cannot occupy the same position in the open 48S PIC and the 80S IC. **(C)** Modeling eIF5B into the closed 48S PIC, in cross-eye stereo. The model was obtained as in panel *(A)*. Only the 18S rRNA and eIF5B from the 80S IC, and Met-tRNA$_i$, eIF2, and eIF1A from the 48S PIC are shown. A steric clash between eIF2 and eIF5B-D4 is evident, although not as extensive as in panel *(B)*, indicating that eIF5B-D4 cannot occupy the same position in the closed 48S PIC and the 80S IC.

A **Modeling the eIF1A-CTT:eIF5B-D4 interaction into the eIF5B:80S IC complex**

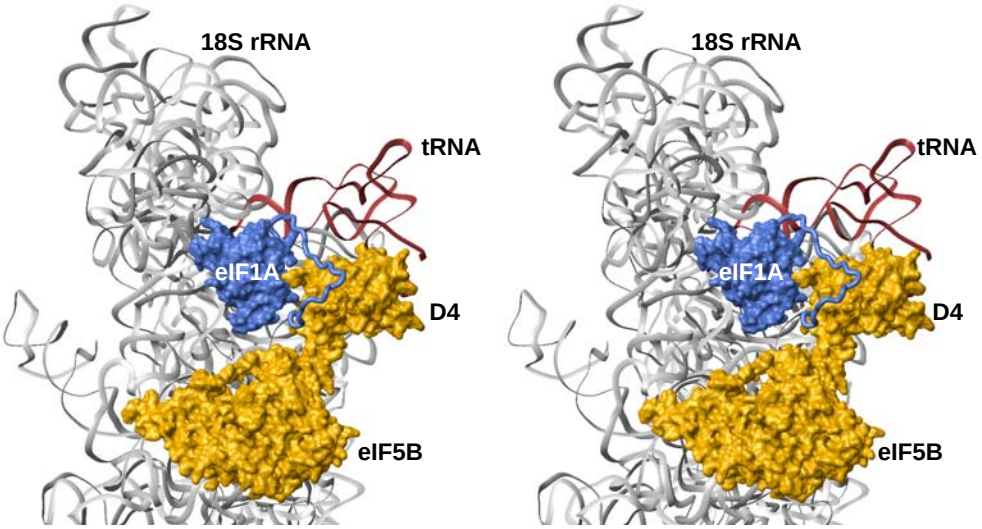

B **Position of eIF1A-CTT when bound to eIF5B-D4 on the ribosome**

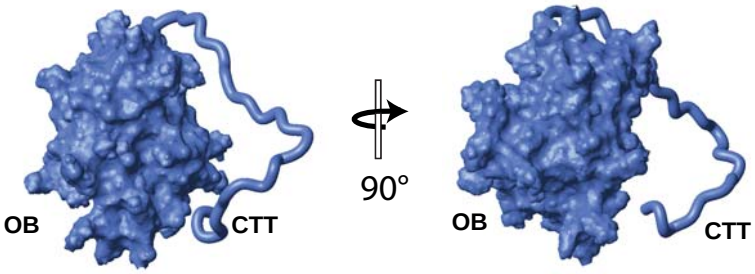

C **Position of eIF1A-CTT in free eIF1A**

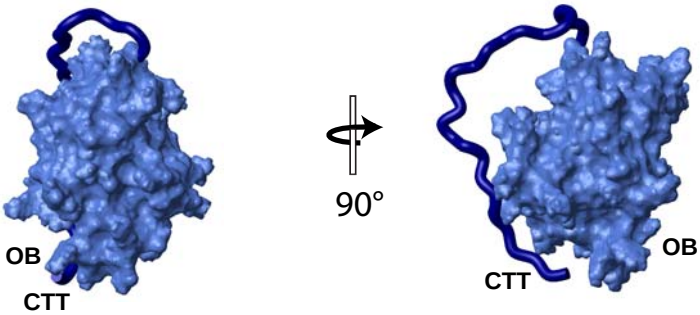

Figure S6. Conformations of eIF1A-CTT on and off the ribosome

(A) Modeling the eIF1A-CTT:eIF5B-D4 interaction into the structure of the eIF5B:80S IC. The model is as in **Fig. S5A**, with the last 11 residues of human eIF1A-CTT (shown as wire) modeled after the crystal structure of the *S. cerevisiae* eIF5B:eIF1A-CTT complex (3wbk.pdb)(Zheng et al. 2014). **(B)** eIF1A from the model in panel *(A)* in the same orientation (left) and rotated 90 degrees (right). eIF1A-CTT is shown as wire; eIF1A-NTT is not shown. **(C)** The model of free eIF1A from **Fig. 2E**, in the same orientation as in panel *(A)* (left) and rotated 90 degrees (right). eIF1A-CTT is shown as wire and colored navy; eIF1A-NTT is not shown. Comparison of the conformations of eIF1A-CTT in free and ribosome-bound eIF1A indicates that it is located on opposite sides of eIF1A-OB and contacts the OB domain in free eIF1A, but not on the ribosome.